Author Manuscript

Author Manuscript

Author Manuscript

Author Manuscript

HHS Public Access

Author manuscript

J Biomed Mater Res A. Author manuscript; available in PMC 2019 June 01.

Published in final edited form as:

J Biomed Mater Res A. 2018 June ; 106(6): 1743–1752. doi:10.1002/jbm.a.36358.

A Thermoresponsive, Citrate-based Macromolecule for Bone Regenerative Engineering[3]

Simona Morochnik[a], **Yunxiao Zhu**[b], **Chongwen Duan**[b], **Michelle Cai**[b], **Russell R. Reid**[c], **Tong-Chuan He**[d], **Jason Koh**[e], **Igal Szleifer**[a,f], and **Guillermo A. Ameer**[a,g]

[a]Biomedical Engineering Department and Chemistry of Life Processes Institute, Northwestern University, Evanston, Illinois, USA

[b]Biomedical Engineering Department, Northwestern University, Evanston, Illinois, USA

[c]Department of Surgery, Plastic and Reconstructive Surgery, The University of Chicago Medical Center, Chicago, IL 60637, USA

[d]Department of Orthopaedic Surgery and Rehabilitation Medicine, The University of Chicago Medical Center, Chicago, IL 60637, USA

[e]NorthShore Orthopaedic Institute, NorthShore University HealthSystem, 2650 Ridge Avenue Suite 2505, Evanston, IL, 60201, USA

[f]Department of Chemistry, Northwestern University, Evanston, Illinois, USA

[g]Department of Surgery, Feinberg School of Medicine, Chicago, Illinois, USA

Abstract

There is a need in orthopaedic and craniomaxillofacial surgeries for materials that are easy to handle and apply to a surgical site, can fill and fully conform to the bone defect, and can promote the formation of new bone tissue. Thermoresponsive polymers that undergo liquid to gel transition at physiological temperature can potentially be used to meet these handling and shape-conforming requirements. However, there are no reports on their capacity to induce *in vivo* bone formation. The objective of this research was to investigate whether the functionalization of the thermoresponsive, antioxidant macromolecule poly(poly-ethyleneglycol citrate-co-N-isopropylacrylamide) (PPCN), with strontium, phosphate, and/or the cyclic RGD peptide would render it a hydrogel with osteoinductive properties. We show that all formulations of functionalized PPCN retain thermoresponsive properties and can induce osteodifferentiation of human mesenchymal stem cells without the need for exogenous osteogenic supplements. PPCN-Sr was the most osteoinductive formulation *in vitro* and produced robust localized mineralization and osteogenesis in subcutaneous and intramuscular tissue in a mouse model. Strontium was not detected in any of the major organs. Our results support the use of functionalized PPCN as a valuable tool for the recruitment, survival, and differentiation of cells critical to the development of new bone and the induction of bone formation *in vivo*.

---

[3]No benefit of any kind will be received either directly or indirectly by the author(s)

Corresponding Author: Guillermo A. Ameer, DSc, Biomedical Engineering Department, Department of Surgery, and Chemistry of Life Processes Institute, Northwestern University, Evanston, Illinois, USA, Phone: (847) 467 - 2992, g-ameer@northwestern.edu.

Supplemental Information: Additional supporting information is included.

Author Manuscript Author Manuscript Author Manuscript Author Manuscript

Keywords

bioengineering; stem cells; fracture healing; bone μCT; matrix mineralization

INTRODUCTION

Cell-matrix interactions have been extensively studied and used as a means to activate signaling cascades implicated in tissue regeneration.[1] These findings have led to the development and investigation of biomaterials to modulate the local chemical, mechanical, and biological microenvironment of cells as a strategy to regenerate tissue and regain function.[2,3] When applying this concept to bone regeneration, the signaling cascades in osteoblasts and osteoclasts must maintain a complex and dynamic balance between bone formation and resorption to generate new bone.[4,5] Furthermore, large bone defects often require viable cells and/or donor tissues to jump-start the process of regeneration.[6,7] Therefore, biomaterials that can: a) function as a temporary scaffold to maximize osteoblast proliferation and differentiation, b) simultaneously minimize bone resorption caused by reactive oxygen species (ROS) generated by osteoclasts, and c) deliver exogenous cells to the patient, could potentially lead to improved bone reconstructive surgery outcomes.

Polymers that form hydrogels are very attractive biomaterials due to their high compatibility with cells and their potential to localize cells and growth factors to a site of interest.[8] We have previously reported the synthesis and characterization of poly(poly-ethyleneglycol citrate-co-N-isopropylacrylamide) (PPCN), a thermoresponsive macromolecule with intrinsic antioxidant properties.[9] We have shown that when PPCN is mixed with 0.1% gelatin, the resulting interpenetrating network supports the differentiation of entrapped cells into osteoblasts and accelerates the healing of a critical-sized craniofacial defect in a mouse.[10] Although the results are very promising, it is desirable to have an off-the-shelf, completely synthetic system that is highly reproducible to eliminate variations in performance due to batch-to-batch heterogeneity typically associated with natural materials such as gelatin. To this end, we investigated the ionic and covalent functionalization of PPCN with Sr^{2+}, $(PO_4)^{3-}$, or the cell adhesion peptide Arg-Gly-Asp (RGD) to engineer PPCN to become osteoinductive and capable of supporting osteogenesis without the need for exogenous osteogenic factors.

Strontium has been shown to increase bone mass by activation of bone-forming osteoblasts and suppression of bone-resorbing osteoclasts.[11,12] Sr^{2+} shares many elemental properties with Ca^{2+} and research has shown the strontium can act via calcium-dependent or independent receptor pathways (CaSRs) to inhibit bone resorption and increase bone formation.[13,14] Despite the restrictions on the oral drug strontium ranelate, recent work by Lourenco et al. has underscored the safety and efficacy of using strontium locally to increase bone formation, namely in 100 mM Sr-doped HA-alginate microspheres.[15] We hypothesized that 100 mM Sr^{2+} can be incorporated into PPCN via the macromolecule's carboxyl groups through ionic or coordination bonds and that the osteoinductive effects can stand alone without HA.

Author Manuscript Author Manuscript Author Manuscript Author Manuscript

Phosphate is another molecule that is critically important for bone formation.[16,17] For example, in the form of β-glycerophosphate, it is a key component of cell culture media to induce osteogenic differentiation *in vitro*. Inorganic phosphate is incorporated into hydroxyapatite as the bone extracellular matrix becomes mineralized—a process that induces osteogenesis.[18,19] Furthermore, it has been shown that the covalent conjugation of phosphate to polyethylene glycol results in scaffolds that are capable of inducing stem cell osteodifferentiation.[20] Therefore, we hypothesized that β-glycerophosphate could be covalently incorporated into the PPCN network and that the resulting macromolecule would have osteoinductive properties.

Finally, peptides that mimic components of the extracellular matrix can modulate cellular processes.[21] Peptide-mediated cell spreading in hydrogels has been shown to promote osteogenic differentiation of stem cells.[22–24] The spatial configuration of the peptide and its presentation to the cell is important because it has been shown that alginate modified with cyclic RGD over linear RGD supported the osteodifferentiation of human mesenchymal stem cells (hMCSs).[25] Although very insightful, earlier studies required osteogenic cell culture media. Herein, we set out to develop a functionalized version of PPCN capable of inducing the osteodifferentiation of stem cells and pre-osteoblasts without the addition of exogenous osteogenic factors. We show that functionalized PPCN retains thermoresponsive gelation properties and can induce mineralization and osteodifferentiation *in vitro and vivo.*

MATERIALS & METHODS

Synthesis and Preparation of PPCN-Sr, PPCN-phos, and PPCN-cRGD

Poly(polyethylene glycol citrate-co-N-isopropylacrylamide) (PPCN) was prepared by polycondensation and subsequent free radical polymerization as previously reported by us.[9] To prepare PPCN-Sr gels, PPCN was dissolved in PBS (1x) at 100 mg/ml. PPCN solutions containing $SrCl_2$ $6H_2O$ (Sigma-Aldrich, St. Louis MO) at a concentration of 100 mM were prepared and left overnight at 4°C prior to use (Scheme S1). This strontium ion concentration was chosen because it induced the highest ALP activity with the least variability in a preliminary optimization study (Fig. S1).[11] To prepare PPCN-phos gels, β-glycerophosphate was added slowly as a powder 10 minutes into the polycondensation step of PPCN synthesis at 0.1 or 0.2 molar ratios to harness the functionality of the reactive hydroxyls of the β-glycerophosphate for reaction with the carboxyls of citric acid (Scheme S2). PPCN-phos of 0.1 molar ratio was chosen for subsequent cell studies because higher molar ratios led to overcrosslinking. The $a_v\beta_3$-receptor integrin binding cyclized RGD thiolated peptide (cyclo-RGDfC; Arg-Gly-Asp-Phe-Cys) was purchased from ABI Scientific (Sterling VA) and covalently conjugated to PPCN via established maleimide-thiol chemistry.[26] Briefly, N-β-maleimidopropionic acid hydrazide (BMPH) (Thermo Fisher Scientific, Waltham MA) was reacted with the carboxyl groups of PPCN using a molar ratio of 0.1 (Scheme S1). The resulting maleimide-functionalized PPCN was reacted with the peptide. The functionality of the synthesized product was confirmed by cell spreading studies shown in Figure 3. PRONOVA™ alginate (Novamatrix, Norway) was prepared at 2% w/v in 10 mM HEPES buffer[11] and used as a control material for cell viability studies.

Author Manuscript Author Manuscript Author Manuscript Author Manuscript

Chemical and Rheological Characterization of Functionalized PPCN

The release of Sr^{2+} from PPCN-Sr was assessed using inductively coupled plasma optical emission spectroscopy (Thermo iCAP 7600 ICP-OES, Thermo Fisher Scientific, Waltham MA) (Fig. 1a). Briefly, PPCN-Sr gels were formed as described above and allowed to gel at 37°C. Subsequently, gels were immersed in pre-warmed simulated body fluid (SBF). Gels were shaken at 40 rpm at 37°C and SBF was collected over a period of 14 days. All of the collected supernatant and the remaining gels were acidified in 2.4% nitric acid and assayed for Sr^{2+} concentration.

PPCN-phos was characterized by Fourier-transform infrared spectroscopy (FT-IR) (Bruker Tensor 37, Billerica MA) (Fig. 1b). Powder samples were prepared using standard KBr pellet preparation and recorded on a spectrometer using an accumulation of 32 scans. X-ray photoelectron spectroscopy (XPS) elemental analysis was conducted in order to confirm the inclusion of phosphate and quantify the ratio of phosphate to carbon, nitrogen and oxygen in the final PPCN-phos formulation (Galbraith Laboratories, Knoxville, TN). Additional characterization is presented in the supplementary information (Fig. S2).

PPCN-cRGD conjugation was confirmed by matrix assisted laser desorption ionization (MALDI-TOF, Bruker) (Fig. 1c). The samples were first dissolved in DI water before mixing with the saturated alpha-cyano-4-hydroxycinnamic acid matrix TFA solution in a 1:1 ratio. The resulting mixture was then pipetted on the sample plate (1 μl in volume) and dried at ambient temperature.

Rheological characterization was carried out on a DHR rheometer (TA Instruments, New Castle DE) with a 20 mm 2° cone peltier plate geometry and solvent trap cover to minimize sample evaporation. All gels were subjected to a temperature ramp experiment from 15°C to 45°C with a heating rate of 5°C/min. The viscoelastic moduli were monitored at an applied angular frequency of 10 rad/s and strain amplitude of 5%. A gap height of 52 μm was used for all samples. The initial change in viscoelastic properties was characterized by an increase of storage modulus (G') over loss modulus (G'').

Antioxidant properties were determined using the 2,2′-azino-bis(3-ethylbenzothiazoline-6-sulphonic acid) (ABTS) radical scavenging decolorization assay.[9] Briefly, an aqueous solution of 7 mM ABTS and 2.45 mM sodium persulfate was prepared at room temperature and incubated in the dark for 16 hours, then filtered with a 0.45 μm filter. Material samples were dissolved in this solution at 50 mg/mL and incubated at 37°C. All materials were tested in triplicate. 50 μL samples of solution were removed at 8 hours; mixed 1:1 with MQ water; and measured for absorbance at 734nm. Activity was measured as % decoloration of ABTS radicals compared to polytetrafluoroethylene (PTFE) negative controls.

In Vitro Evaluation of Functionalized PPCN

i. 3D Cell Culture—Human mesenchymal stem cells (hMSCs, ATCC) were encapsulated in various PPCN, PPCN-Sr, PPCN-phos or PPCN-cRGD solutions of 100 mg/mL PPCN in PBS (1x). Cells were added to the various PPCN formulations at a concentration of 1×10^5 cells/mL liquid PPCN. The cell-PPCN suspension was incubated at 37°C for 5 min to allow gelation. Once the gel was formed, warm cell culture media was added and changed every 2

Author Manuscript Author Manuscript Author Manuscript Author Manuscript

days. Prior to seeding, the plate was coated with Sigmacote (Sigma-Aldrich, St. Louis MO) to prevent cell attachment to the plate, ensuring that all cells remain within the 3D gel. hMCSs were cultured in Dulbecco's Modified Eagle medium (DMEM), 4.5 g/L glucose, and supplemented with 10% FBS and 5 ml 10x penicillin-streptomycin with no further osteogenic supplementation. All hMSCs used in these studies were at passage 6 or below and cultured at 37°C and 5% carbon dioxide (CO_2). During handling, the plates were kept on a plate-warmer to ensure the gel would not liquefy as a result of temperature fluctuations. At each time-point, the media was removed and the gel was collected and either frozen to measure ALP activity and DNA content or assayed directly for cell viability and mineralization.

ii. Assessment of Cell Viability—LIVE/DEAD staining was used to assess cell viability in culture. Calcein AM was used as an indicator of live cells and ethidium homodimer-1 was used as an indicator of dead cells (Thermo Fisher Scientific, Waltham MA). The staining solution was prepared by adding 2 μl of each stain to 1 ml of PBS (1x). Culture media was removed and stain solution was added to the samples. Gels were left to incubate in dark at 37°C for 30 minutes and were subsequently imaged on a Nikon TE-2000U fluorescence microscope. 4–5 images were taken per group and cell viability was determined by counting number of live cells over total cells. Average quantification and representative images of each group are shown.

iii. Assessment of Early Osteodifferentiation—Alkaline phosphatase (ALP) activity was measured according to a fluorometric kit (Biovision, Milpitas CA). At days 3 and 10, the gels were collected, immersed in ALP buffer. A non-fluorescent substrate, 4-Methylumelliferyl phosphate disodium salt (MUP), was added and cleaved by ALP, which results in a fluorescent signal (Ex/Em = 360/440nm). The fluorescence was read on a SpectraMax M3 microplate reader (Molecular Devices, Sunnyvale CA). The enzymatic activity was calculated based on serially diluted gel standards and normalized to total DNA content assessed using the Quant-iT PicoGreen assay (Thermo Fisher Scientific, Waltham MA).

iv. Assessment of Late Osteodifferentiation—Alizarin Red S staining was performed at day 21 according to an established protocol (PromoCell, Heidelberg, Germany). The stain solution was made from Alizarin Red S powder (Sigma-Aldrich, St. Louis MO). The cells were fixed inside the warmed gels and the stain was allowed to permeate gels while excess stain was subsequently rinsed out with several washes of deionized water. Mineralization was visualized with light microscopy. Images were processed with ImageJ and quantified via threshold intensity.

Osteopontin (OPN) and osteocalcin (OCN) expression were assessed via immunohistochemistry at day 21. The primary antibody was prepared as 1:200 dilution in 0.05% BSA/PBS. The secondary antibody was prepared as a 1:500 dilution in 0.05% BSA/PBS. The nuclear counterstain used was bisBenzimide H 33342 (Sigma-Aldrich, St. Louis MO). Fluorescent images were taken by Nikon TE-2000U. 4–5 images were taken per group and percentage of positive expression was quantified as percentage of positively staining cells over total cells. Cells with a positive signal for the stain were identified by comparing

Author Manuscript Author Manuscript Author Manuscript Author Manuscript

experimental wells to control wells to which only secondary antibody was added, omitting primary. Cells that were positive for OPN and OCN were quantified via histomorphometry.

In Vivo Evaluation of Functionalized PPCN

NIH guidelines for the care and use of laboratory animals (NIH Publication #85-23 Rev. 1985) have been observed. All procedures were conducted using protocols approved by Northwestern University's Institutional Animal Care and Use Committee. Ectopic bone formation in the mouse hind limb was used to assess osteoinduction and osteogenesis *in vivo*.[27] Six NU/NU nude male mice (8–10 weeks, Charles River Laboratories) were used for these studies—three in the PPCN control group and three in the experimental PPCN-Sr group. All PPCN formulations were sterilized with ethylene oxide gas. PPCN, PPCN-Sr and hMSCs were prepared separately. Immediately prior to injection, 5×10^5 cells/mL were added to PPCN solutions. The mice were anesthetized with isoflurane (1–3% with oxygen), the injection site was cleaned, and 100 μL of cell-containing solution was injected in two positions on each mouse, subcutaneously near the left femur and intramuscularly near the right femur. After injection, the mice were housed in a designated animal facility (CAMI, Center for Advanced Molecular Imaging) and cared for in compliance with the regulations established by the Northwestern University Institutional Animal Care and Use Committee. Animals were examined for post-operational pain for the first 10 days, specifically for signs of overall animal mobility, eating and drinking habits, changes in body weight, and/or appearance of surgical wounds. The study was carried out for 42 days and animals were imaged at days 0, 10, 21 and 42.

i. Radiographic imaging—To assess mineralization or bone formation, mice were anesthetized with isoflurane and placed on the heated microCT bed. Images were acquired with a preclinical microPET/CT imaging system, nanoScan scanner (Mediso-USA, Boston, MA). Data were acquired with "medium" magnification, 33 μm focal spot, 1 × 1 binning, with 720 projection views over a full circle, with a 300 ms exposure time. Images were acquired using 35 kVp. The projection data were reconstructed with a voxel size of 68 μm using filtered back-projection software from Mediso. The reconstructed data were visualized and segmented in Osirix Lite for Mac. Using the coronal plane, images were quantified by creating regions of interest (ROI) with 2D region-growing using a lower threshold of 600 and an upper threshold of 10,000 Hounsfield units (HU). The regions of interests (ROIs) were used for quantification of mineralization by calculating the mean HU for each ROI (bone is 700 to 3,000 HU).

ii. Tissue processing and Immunofluorescence Assessment—Animals were euthanized by carbon dioxide inhalation and tissues were collected and fixed using 4% paraformaldehyde in PBS overnight at 4°C. Samples were washed with PBS with several changes to remove any residual paraformaldehyde. The samples were dehydrated by series of ethanol solutions, cleared by xylene, and embedded in paraffin. Sections of 5-micron thickness were cut and mounted on slides. Sections were treated by xylene to remove paraffin, hydrated by alternating ethanol and water. Slides were immersed into antigen retrieval buffer (10 mM Sodium citrate, 0.05% Tween 20, pH 6.0) and heated at 100°C for 15 min. After washing with PBS, the samples were blocked using 5 mg/mL BSA, 5%

Author Manuscript Author Manuscript Author Manuscript Author Manuscript

normal goat serum in PBS for 30 min. Samples were incubated with primary antibody diluted in blocking buffer at 4°C overnight. Slides were then washed by PBS 3 × 5 min and incubated with secondary antibody diluted by blocking buffer at room temperature for 30 min. Slides were washed by PBS 6 × 5 min, then mounted with anti-fade medium and sealed with nail polish. Images were taken with a Nikon TE-2000U microscope or a Cytation5 image reader (BioTek Instruments, Winooski VT).

iii. Determination of Strontium Distribution—The presence of strontium was measured in the heart, brain, spleen, testes, muscle, lung, kidney, and liver. After euthanizing the animals, each organ was collected and stored at −80°C until analysis. Tissue digestion was carried out by adding 70% nitric acid and 37% hydrogen peroxide to each sample. Samples were uncapped after 1 hour to release built up gas. Tissues were left to digest for 2 days at room temperature. After 2 days, the samples were diluted down to 2.4% acid in MQ water and prepared for ICP-OES as described above.

iv. Elemental Analysis—XPS analysis of the sectioned tissue was conducted on a Thermo Fisher ESCALab 250Xi using Al K-alpha X-ray source (1486.6 eV) (Thermo Fisher Scientific, Waltham MA). The monochromated X-ray beam spot size was 300 μm in diameter and the power was 100 watts. A pass energy of 100 eV and step size of 1 eV were used for the survey scan. For the high resolution scan, 50 eV of pass energy and a 0.1 eV step size were used. The dwell time was 50 ms. The XPS spectra were calibrated with adventitious carbon peak at 284.8 eV. All XPS data were processed with Avantage software.

Statistical Analysis

Statistical analysis was performed with Microsoft Excel software and GraphPad Prism 6.0 (GraphPad Software Inc., La Jolla CA). Analysis of variance was carried out with independent sample T-tests for ALP, Alizarin Red S, immunohistochemistry and mineralization data. A value of $p < 0.05$ was considered significant.

RESULTS

Strontium, phosphates, and the peptide cRGD can be tethered within PPCN

Characterization of PPCN-Sr by ICP-OES confirms the successful entrapment and release of Sr^{2+}. The strontium is slowly released within 7 days (Fig. 1a). FT-IR characterization of PPCN-phos shows growth of a peak associated with phosphate at 1116 nm^{-1} that is indicative of the P=O phosphate stretch and broadening around 3400 nm^{-1} indicative of the OH associated with this phosphate (Fig. 1b). Additionally, it shows growth of a peak at 1238 nm^{-1} that is absent in the spectrum of β-glycerophosphate. Elemental analysis corroborates the inclusion of phosphate. Confirmation of phosphate incorporation into the PPCN backbone is shown in supplementary information by evaluating the effect of mixtures of PPCN and phosphates versus covalently incorporated phosphates on ALP activity (Fig. S3). Covalent conjugation of cRGD to PPCN carboxylic acid groups was confirmed by the MALDI spectra (Fig. 1c). Signature peaks of cRGD + BMPH and cRGD + BMPH + citric acid were easily identifiable, confirming the successful conjugation of the peptide to PPCN. cyclic-RGD has a molecular weight of 578.7 g/mol. In this spectrum, it appears with three

Author Manuscript Author Manuscript Author Manuscript Author Manuscript

additional protons and fragments at 581.7 m/z. The full monomer also appears at 1156 m/z as expected. Rheological characterization confirmed that the thermoresponsive behavior of the functionalized PPCN is maintained as crossover points for the loss and storage moduli are present (Fig. 2). The lower critical solution temperatures (LCST) for PPCN-Sr, PPCN-phos, and PPCN-cRGD were 28.5°C, 28.5°C, and 22.2°C, respectively.

Cells Entrapped in Functionalized PPCN Remain Viable and Undergo Osteodifferentiation

According to LIVE/DEAD staining, all of the PPCN formulations support the viability of hMSCs (Fig. 3). The morphology of cells entrapped in PPCN-Sr and PPCN-phos hydrogels was mostly rounded whereas cells entrapped in PPCN-cRGD exhibited an elongated or spread morphology, consistent with integrin-dependent binding activity. Though hMSCs entrapped in functionalized PPCN formulations did not exhibit significant alkaline phosphatase (ALP) activity at early timepoints, they all exhibited late-stage osteodifferentiation. For the hMSCs, the PPCN-Sr group shows an initial burst of enhanced ALP activity at day 3 with no significant difference in ALP among groups at day 10 (Fig. 4). All three functionalized PPCN formulations supported the osteodifferentiation of hMSCs at day 21 when compared to TCP and PPCN controls (Fig. 5). Cells in PPCN did not show any signs of mineralization. The PPCN-Sr group exhibited the greatest extent of mineralization and OPN expression. All three functionalized variants show significant OPN and OCN expression relative to the TCP control. However, PPCN-Sr was chosen for the *in vivo* experiments due to overall superior performance in the *in vitro* osteodifferentiation studies.

PPCN-Sr induces mineralization *in vivo* and Sr is locally cleared

PPCN-Sr with hMSCs was successfully injected both intramuscularly and subcutaneously near femurs of nude mice. According to microCT images and quantification, bone formation or mineralization was most evident at the intramuscular injection sites (Fig. 6) although the subcutaneous mineralization is presented in the supplement (Fig. S4). As strontium is radiopaque, the initial injection volume is slightly detectable at day 0. However, at each time-point evaluated, the region of mineralization grows, distinctly separate from the femur of the mouse. By day 42, the average mineralized region for all PPCN-Sr mice is approximately 38.9 mm^3. For non-functionalized PPCN, there is no mineralization detected at any time-point. Tissue sections were positive for osteocalcin and mineralization in all PPCN-Sr injection sites (Figs. 7, S5). There was no evidence of strontium in any of tissue sections or the main organs, while calcium was readily detected in tissue sections from the PPCN-Sr injection sites (Fig. S6, 7).

DISCUSSION

The ability to rapidly induce localized bone formation without side effects is a highly desired capability that to date remains elusive. Combining this property with a material that is shape-conforming and antioxidant is very advantageous for many orthopedic and craniomaxillofacial surgeries that contain irregular defects and heightened local inflammation. Herein, we describe the synthesis and characterization of three formulations of an injectable, phase changing, citrate-based macromolecule that is suitable to induce bone formation. These formulations, PPCN-cRGD, PPCN-Sr, and PPCN-phos maintained their

Author Manuscript Author Manuscript Author Manuscript Author Manuscript

thermoresponsive behavior at physiologically relevant temperatures. The LCST of PPCN-cRGD had the largest shift from that of PPCN likely due to the hydrophobicity the peptide adds to the polymer network. This effect of peptides on the LCST has been documented previously for copolymers of poly(N isopropylacrylamide) (PNIPAAm) and polyethylene glycol (PEG).[28,29] Hydrophobic units may accentuate the hydrophobic effect of NIPAAm collapse leading to reduced hydrogen bonding between the polymer and solvent at elevated temperatures. Additionally, we show that the formulation with the best *in vitro* osteoinductivity, PPCN-Sr, maintained the antioxidant properties of PPCN previously reported by us.[9] Polydiolcitrates have previously been reported to scavenge free radicals and PPCN-Sr corroborates this property.[30,31] PPCN-Sr demonstrated elevated radical scavenging abilities via an ABTS assay, with almost 50% of the free radicals scavenged in 8 hours (Fig. S7).

Our results also show that cell spreading is not a necessary early step for osteodifferentiation to take place. PPCN-Sr and PPCN-phos groups that lack the RGD moiety, which impairs the ability for the cells to initially spread within the hydrogel, still support osteodifferentiation with rounded cell morphologies. Cyclic RGD peptides are highly selective toward the $a_v\beta_3$ receptor, which activates the osteoblast specific transcription factor runt-related transcription factor 2 (RUNX2) via FAK signaling during osteogenesis.[32] However, the FAK pathway is just one of many pathways toward RUNX2 activation—others include wnt/catenin signaling and PLC signaling activated by Ca^{2+} via calcium sensing receptors.[33,34] Our results underscore the utility of targeting these alternative pathways and show that while RGD-induced cell spreading is one method of activing RUNX2, cell spreading itself may not be not essential for osteodifferentiation.

Finally, our PPCN-Sr system serves as a novel, injectable and antioxidant system to induce bone formation. A recent literature review found that, among 27 studies examining Sr-biomaterial effects in *in vivo* bone formation, Sr amounts ranged widely from 0.1 wt% to 22 wt%.[35] As a point of comparison, our 100 mM Sr concentration translates to 2.4 wt%. This is in the lower range of concentrations used by others, which underscores the value of the mineralization that we began to detect as early as day 10. Notably, the study that used the lowest amount, 0.1 wt% evaluated bone formation at 60 days.[36] As our study was preliminary, we only evaluated bone formation through 42 days. Our future work in this area involves extending our *in vivo* study to longer timescales and evaluating lower strontium concentrations. Preliminary ALP activity data suggests we can reduce our concentration of strontium to approximately 1 wt% or less in future work.

Our PPCN-Sr system also builds on the work of other studies by offering dual injectability and antioxidant activity. A prior concern for strontium use clinically has been the significant yet small risk of myocardial infarction associated with the oral drug strontium ranelate.[37] To avoid this concern, we develop an injectable system that localizes the strontium to the injection site. No strontium was found in any of the tissues that were assessed at day 42. This underscores the local release and clearance of strontium from the site and encourages the case for PPCN-Sr as a safe macromolecule clinically. Of the *in vivo* Sr-biomaterial literature, only 2 studies used injectable systems and none of the materials were inherently antioxidant—the first was the study by Lourenco et al which employed 100 mM Sr-doped

Author Manuscript Author Manuscript Author Manuscript Author Manuscript

HA-alginate microspheres and the second incorporated 9 mol % SrO in borate bioactive glass.[15,38] The majority of the other materials used were calcium phosphate-based, doped with HA, or variants of bioactive glass.[39–43] We present PPCN-Sr as a superior material in demonstrating that 100 mM of Sr incorporated in PPCN can generate bone formation without the inclusion of HA, while simultaneously avoiding the brittleness of bioactive glass.[44] Thus, to the best of our knowledge, PPCN-Sr is not only an excellent, osteoinductive, injectable macromolecule but also the first inherently antioxidant macromolecule for bone regeneration.

Although the results of our study are very encouraging, there are some limitations that we address. The number of hMSC used for each injection for the *in vivo* experiments is relatively low, explaining the limited formation of trabecular bone in the tissue. Another limitation is the ectopic bone formation model that was used, which although appropriate as a screening tool, may not be indicative of how the material will perform in a bone defect. However, data not included here suggest that PPCN-Sr without any hMSCs may be sufficient to induce mineralization. Future work will focus on a dose response study with the number of injected hMSCs in the PPCN-Sr and the impact of lower Sr^{2+} concentrations in the PPCN *in vivo*. We will also investigate the best performing formulation in a bone defect model in order to better understand the potential of this approach for bone regenerative engineering.

Supplementary Material

Refer to Web version on PubMed Central for supplementary material.

Acknowledgments

This research was supported by the NIH Chemistry of Life Processes Pre-doctoral Training Grant under Award #5T32GM105538-03. Special thank you to Drs. Chad Haney and Alex Waters of the Center for Advanced Molecular Imaging (CAMI) at Northwestern University for assisting with radiographic imaging and assessment.

References

1. Hay, ED. Cell biology of extracellular matrix. New York: Plenum Press; 1981. p. xvp. 417-1.leaf of plates p
2. Lutolf MP, Hubbell JA. Synthetic biomaterials as instructive extracellular microenvironments for morphogenesis in tissue engineering. Nature Biotechnology. 2005; 23(1):47–55.
3. Kim BS, Mooney DJ. Development of biocompatible synthetic extracellular matrices for tissue engineering. Trends in Biotechnology. 1998; 16(5):224–230. [PubMed: 9621462]
4. Robling AG, Castillo AB, Turner CH. Biomechanical and molecular regulation of bone remodeling. Annu Rev Biomed Eng. 2006; 8:455–98. [PubMed: 16834564]
5. Weilbaecher KN, Guise TA, McCauley LK. Cancer to bone: a fatal attraction. Nat Rev Cancer. 2011; 11(6):411–25. [PubMed: 21593787]
6. Bruder SP, Fink DJ, Caplan AI. Mesenchymal Stem-Cells in in Bone-Development, Bone Repair, and Skeletal Regeneration Therapy. Journal of Cellular Biochemistry. 1994; 56(3):283–294. [PubMed: 7876320]
7. Bianco P, Robey PG. Stem cells in tissue engineering. Nature. 2001; 414(6859):118–21. [PubMed: 11689957]
8. Zhu J, Marchant RE. Design properties of hydrogel tissue-engineering scaffolds. Expert Rev Med Devices. 2011; 8(5):607–26. [PubMed: 22026626]

Author Manuscript Author Manuscript Author Manuscript Author Manuscript

9. Yang J, van Lith R, Baler K, Hoshi RA, Ameer GA. A Thermoresponsive Biodegradable Polymer with Intrinsic Antioxidant Properties. Biomacromolecules. 2014; 15(11):3942–3952. [PubMed: 25295411]
10. Dumanian ZP, Tollemar V, Ye J, Lu M, Zhu Y, Liao J, Ameer GA, He TC, Reid RR. Repair of critical sized cranial defects with BMP9-transduced calvarial cells delivered in a thermoresponsive scaffold. PLoS One. 2017; 12(3):e0172327. [PubMed: 28249039]
11. Place ES, Rojo L, Gentleman E, Sardinha JP, Stevens MM. Strontium- and zinc-alginate hydrogels for bone tissue engineering. Tissue Eng Part A. 2011; 17(21–22):2713–22. [PubMed: 21682547]
12. Bonnelye E, Chabadel A, Saltel F, Jurdic P. Dual effect of strontium ranelate: stimulation of osteoblast differentiation and inhibition of osteoclast formation and resorption in vitro. Bone. 2008; 42(1):129–38. [PubMed: 17945546]
13. Fromigue O, Hay E, Barbara A, Petrel C, Traiffort E, Ruat M, Marie PJ. Calcium sensing receptor-dependent and receptor-independent activation of osteoblast replication and survival by strontium ranelate. J Cell Mol Med. 2009; 13(8B):2189–99. [PubMed: 20141614]
14. Hurtel-Lemaire AS, Mentaverri R, Caudrillier A, Cournarie F, Wattel A, Kamel S, Terwilliger EF, Brown EM, Brazier M. The calcium-sensing receptor is involved in strontium ranelate-induced osteoclast apoptosis. New insights into the associated signaling pathways J Biol Chem. 2009; 284(1):575–84. [PubMed: 18927086]
15. Henriques Lourenco A, Neves N, Ribeiro-Machado C, Sousa SR, Lamghari M, Barrias CC, Trigo Cabral A, Barbosa MA, Ribeiro CC. Injectable hybrid system for strontium local delivery promotes bone regeneration in a rat critical-sized defect model. Sci Rep. 2017; 7(1):5098. [PubMed: 28698571]
16. Chang YL, Stanford CM, Keller JC. Calcium and phosphate supplementation promotes bone cell mineralization: implications for hydroxyapatite (HA)-enhanced bone formation. J Biomed Mater Res. 2000; 52(2):270–8. [PubMed: 10951365]
17. Glimcher MJ. Bone: Nature of the Calcium Phosphate Crystals and Cellular, Structural, and Physical Chemical Mechanisms in Their Formation. Reviews in Mineralogy and Geochemistry. 2006; 64(1):223–282.
18. Boskey AL, Guidon P, Doty SB, Stiner D, Leboy P, Binderman I. The mechanism of beta-glycerophosphate action in mineralizing chick limb-bud mesenchymal cell cultures. J Bone Miner Res. 1996; 11(11):1694–702. [PubMed: 8915777]
19. Chung CH, Golub EE, Forbes E, Tokuoka T, Shapiro IM. Mechanism of action of beta-glycerophosphate on bone cell mineralization. Calcif Tissue Int. 1992; 51(4):305–11. [PubMed: 1422975]
20. Benoit DS, Schwartz MP, Durney AR, Anseth KS. Small functional groups for controlled differentiation of hydrogel-encapsulated human mesenchymal stem cells. Nat Mater. 2008; 7(10): 816–23. [PubMed: 18724374]
21. Wei Q, Pohl TL, Seckinger A, Spatz JP, Cavalcanti-Adam EA. Regulation of integrin and growth factor signaling in biomaterials for osteodifferentiation. Beilstein J Org Chem. 2015; 11:773–83. [PubMed: 26124879]
22. Dalby MJ, Gadegaard N, Oreffo RO. Harnessing nanotopography and integrin-matrix interactions to influence stem cell fate. Nat Mater. 2014; 13(6):558–69. [PubMed: 24845995]
23. Giancotti FG, Tarone G. Positional control of cell fate through joint integrin/receptor protein kinase signaling. Annu Rev Cell Dev Biol. 2003; 19:173–206. [PubMed: 14570568]
24. Rowley JA, Madlambayan G, Mooney DJ. Alginate hydrogels as synthetic extracellular matrix materials. Biomaterials. 1999; 20(1):45–53. [PubMed: 9916770]
25. Hsiong SX, Boontheekul T, Huebsch N, Mooney DJ. Cyclic arginine-glycine-aspartate peptides enhance three-dimensional stem cell osteogenic differentiation. Tissue Eng Part A. 2009; 15(2): 263–72. [PubMed: 18783323]
26. Ravi S, Krishnamurthy VR, Caves JM, Haller CA, Chaikof EL. Maleimide-thiol coupling of a bioactive peptide to an elastin-like protein polymer. Acta Biomater. 2012; 8(2):627–35. [PubMed: 22061108]
27. Scott MA, Levi B, Askarinam A, Nguyen A, Rackohn T, Ting K, Soo C, James AW. Brief review of models of ectopic bone formation. Stem Cells Dev. 2012; 21(5):655–67. [PubMed: 22085228]

Author Manuscript Author Manuscript Author Manuscript Author Manuscript

28. Lutz J-F, Hoth A. Preparation of Ideal PEG Analogues with a Tunable Thermosensitivity by Controlled Radical Copolymerization of 2-(2-Methoxyethoxy)ethyl Methacrylate and Oligo(ethylene glycol) Methacrylate. Macromolecules. 2006; 39(2):893–896.
29. Jain K, Vedarajan R, Watanabe M, Ishikiriyama M, Matsumi N. Tunable LCST behavior of poly(N-isopropylacrylamide/ionic liquid) copolymers. Polymer Chemistry. 2015; 6(38):6819–6825.
30. van Lith R, Gregory EK, Yang J, Kibbe MR, Ameer GA. Engineering biodegradable polyester elastomers with antioxidant properties to attenuate oxidative stress in tissues. Biomaterials. 2014; 35(28):8113–22. [PubMed: 24976244]
31. van Lith R, Wang X, Ameer G. Biodegradable Elastomers with Antioxidant and Retinoid-like Properties. ACS Biomater Sci Eng. 2016; 2(2):268–277. [PubMed: 27347559]
32. Schneider GB, Zaharias R, Stanford C. Osteoblast integrin adhesion and signaling regulate mineralization. J Dent Res. 2001; 80(6):1540–4. [PubMed: 11499509]
33. Papachroni KK, Karatzas DN, Papavassiliou KA, Basdra EK, Papavassiliou AG. Mechanotransduction in osteoblast regulation and bone disease. Trends Mol Med. 2009; 15(5): 208–16. [PubMed: 19362057]
34. Yang F, Yang D, Tu J, Zheng Q, Cai L, Wang L. Strontium enhances osteogenic differentiation of mesenchymal stem cells and in vivo bone formation by activating Wnt/catenin signaling. Stem Cells. 2011; 29(6):981–91. [PubMed: 21563277]
35. Neves N, Linhares D, Costa G, Ribeiro CC, Barbosa MA. In vivo and clinical application of strontium-enriched biomaterials for bone regeneration: A systematic review. Bone Joint Res. 2017; 6(6):366–375. [PubMed: 28600382]
36. Jebahi S, Oudadesse H, El Feki H, Rebai T, Keskes H, Pellen-Mussi P, El Feki A. Antioxidative/oxidative effects of strontium-doped bioactive glass as bone graft. In vivo assays in ovariectomised rats Journal of Applied Biomedicine. 2012; 10(4):195–209.
37. Reginster JY, Neuprez A, Dardenne N, Beaudart C, Emonts P, Bruyere O. Efficacy and safety of currently marketed anti-osteoporosis medications. Best Pract Res Clin Endocrinol Metab. 2014; 28(6):809–34. [PubMed: 25432354]
38. Zhang Y, Cui X, Zhao S, Wang H, Rahaman MN, Liu Z, Huang W, Zhang C. Evaluation of injectable strontium-containing borate bioactive glass cement with enhanced osteogenic capacity in a critical-sized rabbit femoral condyle defect model. ACS Appl Mater Interfaces. 2015; 7(4): 2393–403. [PubMed: 25591177]
39. Baier M, Staudt P, Klein R, Sommer U, Wenz R, Grafe I, Meeder PJ, Nawroth PP, Kasperk C. Strontium enhances osseointegration of calcium phosphate cement: a histomorphometric pilot study in ovariectomized rats. J Orthop Surg Res. 2013; 8:16. [PubMed: 23758869]
40. Hulsart-Billstrom G, Xia W, Pankotai E, Weszl M, Carlsson E, Forster-Horvath C, Larsson S, Engqvist H, Lacza Z. Osteogenic potential of Sr-doped calcium phosphate hollow spheres in vitro and in vivo. J Biomed Mater Res A. 2013; 101(8):2322–31. [PubMed: 23359485]
41. Thormann U, Ray S, Sommer U, Elkhassawna T, Rehling T, Hundgeburth M, Henss A, Rohnke M, Janek J, Lips KS, et al. Bone formation induced by strontium modified calcium phosphate cement in critical-size metaphyseal fracture defects in ovariectomized rats. Biomaterials. 2013; 34(34): 8589–98. [PubMed: 23906515]
42. Boyd D, Carroll G, Towler MR, Freeman C, Farthing P, Brook IM. Preliminary investigation of novel bone graft substitutes based on strontium-calcium-zinc-silicate glasses. J Mater Sci Mater Med. 2009; 20(1):413–20. [PubMed: 18839286]
43. Gorustovich AA, Steimetz T, Cabrini RL, Porto Lopez JM. Osteoconductivity of strontium-doped bioactive glass particles: a histomorphometric study in rats. J Biomed Mater Res A. 2010; 92(1): 232–7. [PubMed: 19172615]
44. Rahaman MN, Day DE, Bal BS, Fu Q, Jung SB, Bonewald LF, Tomsia AP. Bioactive glass in tissue engineering. Acta Biomater. 2011; 7(6):2355–73. [PubMed: 21421084]

Author Manuscript Author Manuscript Author Manuscript Author Manuscript

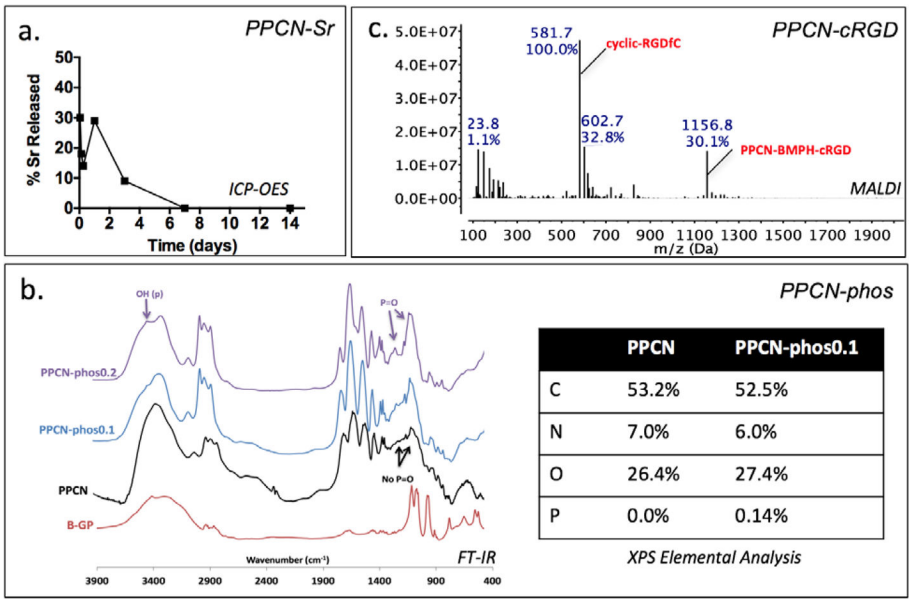

Figure 1.

(a) ICP-OES of 100 mM Sr^{2+} release from PPCN-Sr gels reveals majority of strontium is released in one week. (b) FT-IR of PPCN-phos shows growth of peaks associated with reagent β-glycerophosphate, namely the broadening of the OH stretch at 3400 nm^{-1} and growth of a new peak around 1238 nm^{-1} attributed to phosphonate. Elemental analysis corroborates this data with a small reduction in carbon due to the displacement of carbon-rich PEG chains by β-glycerophosphate. (c) MALDI spectrum of PPCN-cRGD major peaks include expected ionized cyclic-RGDfC at 581.7 m/z and full monomer at 1156 m/z.

Author Manuscript Author Manuscript Author Manuscript Author Manuscript

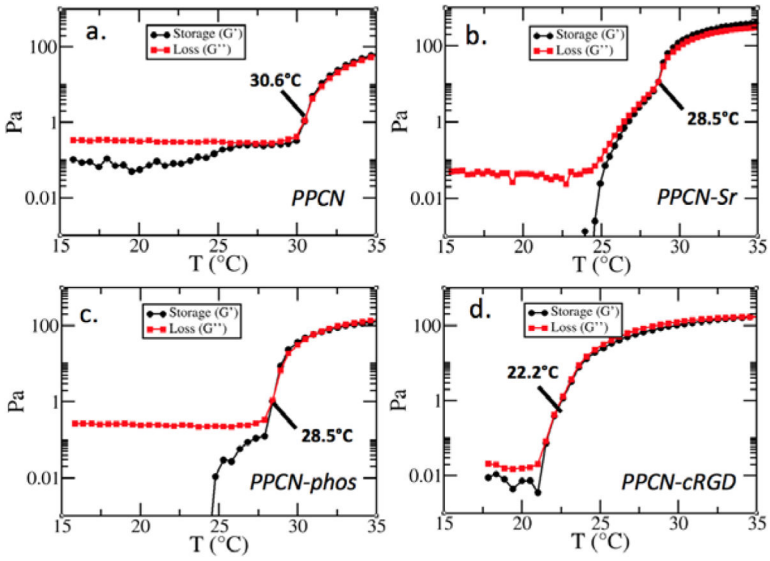

Figure 2.

Rheological characterization of PPCN (a) as compared to PPCN-Sr (b), PPCN-phos (c) and PPCN-cRGD (d) confirms that all three osteoinductive variants maintain thermoresponsive behavior and exhibit a lower LCST transition than PPCN.

Author Manuscript Author Manuscript Author Manuscript Author Manuscript

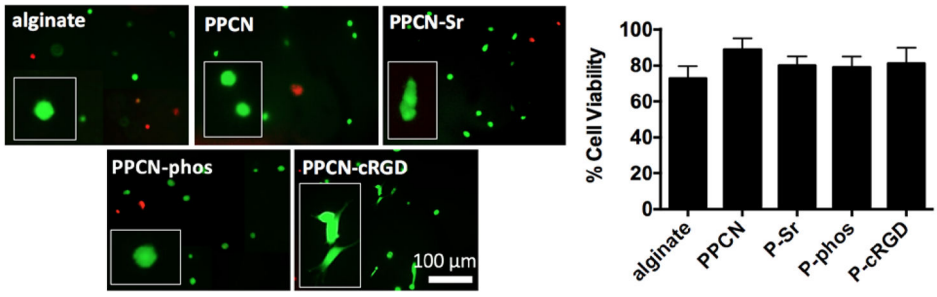

Figure 3.

LIVE/DEAD imaging of hMSCs seeded in 3D gels and cultured in regular DMEM. Cells were seeded in either alginate, PPCN, PPCN-cRGD, PPCN-Sr, or PPCN-phos gels. Cells grown in PPCN-cRGD gels show spreading morphology confirming the functionality of RGD is preserved post-conjugation. Viability in all gels is above 75%. Images were taken at day 10 and representative images shown from $n = 3$ wells.

Author Manuscript Author Manuscript Author Manuscript Author Manuscript

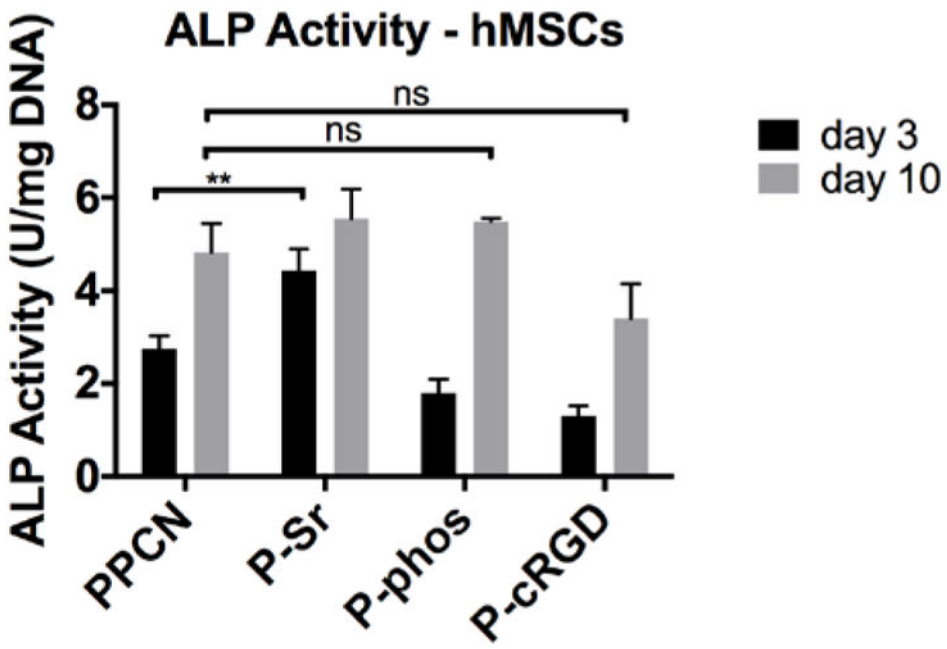

Figure 4.

Day 3 and 10 alkaline phosphatase (ALP) activity shown for hMSCs. hMSCs seeded in PPCN-Sr show a burst of ALP activity at day 3 but no significant increase in ALP is detected for hMSCs as compared to PPCN at day 10. ** *P*-value<0.01.

Author Manuscript Author Manuscript Author Manuscript Author Manuscript

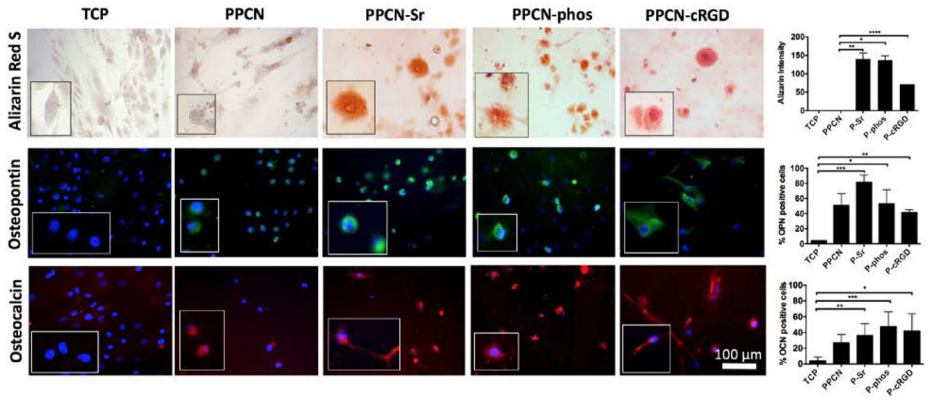

Figure 5.

Characterization of hMSCs at day 21 via staining for calcium deposition by Alizarin Red S, immunohistochemistry for osteopontin (OPN), and osteocalcin (OCN). Corresponding quantification is shown on the right. Mineralization is seen in all three functionalized groups. Osteopontin expression is highest in PPCN-Sr and osteocalcin expression is highest in PPCN-phos. Representative images shown from each group, n = 4. **P*-value<0.05 and ***P*-value<0.01

Author Manuscript Author Manuscript Author Manuscript Author Manuscript

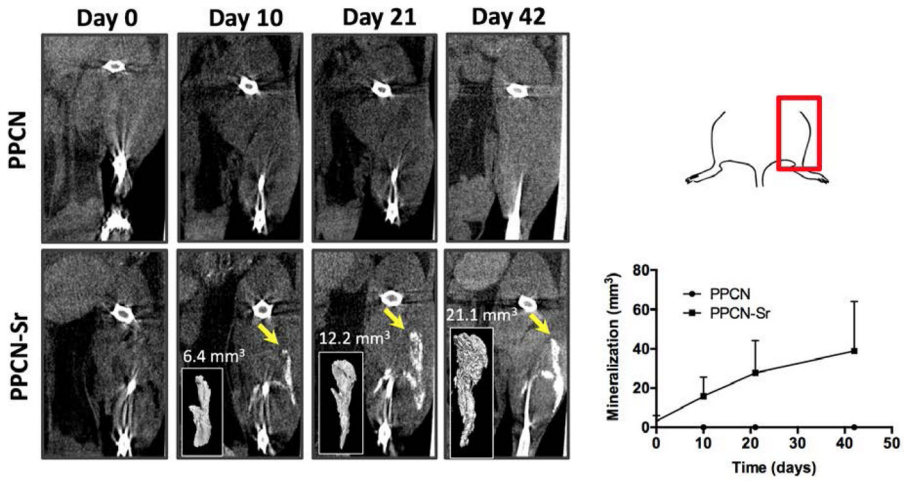

Figure 6.

MicroCT analysis of intramuscular femoral injection of PPCN and PPCN-Sr is shown from day 0 to day 42. The top right panel orients the microCT images onto the mouse femur. The bottom right panel shows the quantification of the microCT images, n = 3. Mineralization is observed in the PPCN-Sr group beginning at day 10 and increasing consistently through the 6 week period. No mineralization is observed in the non-functionalized PPCN control. Mineralized regions were quantified with Osirix by threshold intensity and reconstructed to show the 3D inlay.

Author Manuscript Author Manuscript Author Manuscript Author Manuscript

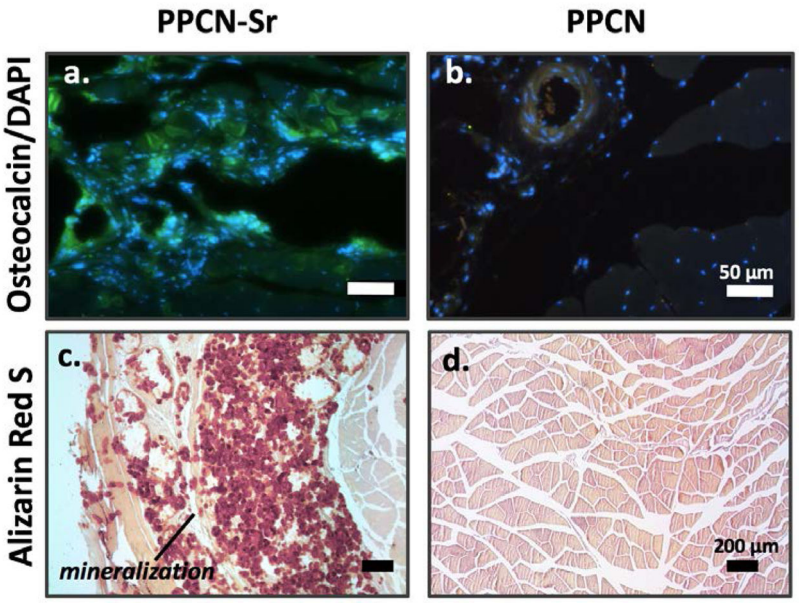

Figure 7.

PPCN-Sr demonstrates significant osteocalcin expression and cell infiltration (a) as compared to PPCN control (b). Alizarin Red S staining for mineralization also demonstrates robust mineralization in PPCN-Sr (c) as detected by red calcium deposits compared to non-functionalized PPCN (d).

Author Manuscript Author Manuscript Author Manuscript Author Manuscript

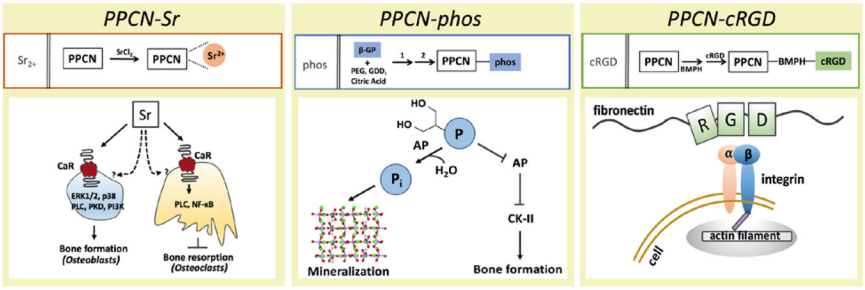

Scheme 1.

Mechanistic schemes of the PPCN formulations explored in this work provides precedent for each of the functionalizations selected. Strontium acts through both dependent and independent CaR (calcium sensing receptor) pathways for osteoblasts and osteoclasts, phosphate acts via both AP (alkaline phosphatase) hydrolysis and via inhibitory AP signaling to stimulate bone formation, and RGD acts through integrin signaling to induce cell spreading and osteodifferentiation.